

Effect of Temperature on Physical and Electrochemical Properties of the Monolithic Carbon-Based Bamboo Leaf to Enhanced Surface Area and Specific Capacitance of the Supercapacitor

B. Armynah^{1,2}, E. Taer³, Z. Djafar¹, Wahyu H. Piarah¹, D. Tahir^{2,*},

¹ Departement of Mechanical Engineering, Hasanuddin University, Bantumarannu Goa 92171 Indonesia

² Departement of Physics, Hasanuddin University, Tamalanrea Makassar 90245 Indonesia

³ Department of Physics, University of Riau, 28293 Simpang Baru, Riau, Indonesia

*E-mail: dtahir@fmipa.unhas.ac.id

Received: 2 April 2019 / Accepted: 25 May 2019 / Published: 30 June 2019

Several analysis have been conducted on the physical and electrochemical properties of monolithic carbon-based bamboo leaf for supercapacitor application. Therefore, the main focus of this study was to analyze the relationship between pore diameter, surface area, and specific capacitance. The variations of pore diameter were found using the activation temperature in the range of 750 °C, 800 °C, 850 °C, and 900 °C. The carbon electrode was prepared in the monolithic form to ensure there is no disturbance with the natural pore of the electrode in the presence of adhesives. The physical properties analyzed include (i) thermal properties, (ii) surface morphology, (iii) elemental content (iv) crystallinity properties and (v) N₂ gas adsorption-desorption isotherm. Furthermore, the specific capacitance was determined through the use of Cyclic Voltammetry (CV) as the electrochemical characteristic. It was discovered that the specific capacitance varies with average pore diameter such that a higher specific capacitance was found with pore diameters smaller than 1.5 nm and the value increased with the size. This research was supported by analysis of surface morphology, elemental content, thermal resistance, and degree of crystallinity.

Keywords: bamboo leaf; activated carbon; biomass

1. INTRODUCTION

The electrochemical double layer capacitor (EDLC) model is a family of electrode storage devices known as supercapacitors. The energy storage process in these devices occurs through the formation of different charge layers at the interface of the electrode and electrolytes in the micropores

of the carbon electrode [1]. The energy stored in the electric field of the devices is simply formulated to be proportional to the capacitance and potential square such that the capacitance is directly proportional to the charge stored and inversely proportional to the potential. From this, it can be ascertained that the formation of more layers of charge leads to higher capacitance and energy to be stored. Geometrically, the capacitance is said to be directly proportional to the surface area of the electrode and inversely proportional to the distance between the two layers of charge formed. However, research on electrodes supercapacitor from carbon materials is still evaluating the relationship between surface area and the distance between two layers of charge to get the optimum combination [2,3,4]. Huang, *et. al* in 2008 examined the relationship of capacitance with pore size for pore distribution varying from 0.7 nm to 50 nm to replace the EDLC model [5]. The results obtained show pores smaller than 1 nm tends to lead to an electric wire-in-cylinder capacitor (EWCC) model, the capacitance increases significantly with the reduction in pore diameter and for those in range of 2-5 nm, the value increases slowly following the electric double-cylinder capacitor (EDCC) model. The 1-2 nm pore range did not display any specific model and was not discussed in detail. Therefore, this study was conducted to show the relationship between surface area and average pore diameter in the range of 1.29-1.66 nm. The variations in pore distribution and surface area were conducted with different physical activation temperature. Furthermore, carbon electrodes were produced from bamboo leaves without the addition of adhesive materials to eliminate the interference with the natural pores. However, physical and electrochemical characterization is explained in the next section.

2. EXPERIMENTAL METHOD

2.1. Preparation of bamboo leaf activated carbon electrodes

Bamboo leaf waste was collected from the Wajo Regency, South Sulawesi. It was washed, dried, cut, and separated from the leaf stalks. Fine pieces samples were pre-carbonized using the low-temperature furnace for 2 hours at a temperature of 200 °C. The pre-carbonized samples were ground using a blender and sieved using a 170-sized mesh. The resulting powder was chemically activated through the use of 0.5 M KOH and washed repeatedly by copious of distilled water until the washing water becomes neutral (pH = 7). The neutral samples were dried at a temperature of 110 °C for 2 days. After this, they were used to form pellets by using the hydraulic press with a compression pressure of 8 tons. This was followed by a single step carbonization-physical activation process through the use of Payun Tech Er-5.2L furnace at a temperature of 600 °C in the N₂ gas environment [6]. A physical activation process was conducted through the use of CO₂ gas at temperatures of 750 °C, 800 °C, 850 °C and 900 °C for 2.5 hours and the samples were labeled BL750, BL800, BL850, and BL900, respectively. The detail preparation of the sample is as shown in Figure 1.

2.2. Physical characterization

The physical properties characterization for carbon electrodes from bamboo leaf waste includes (i) thermal properties, (ii) surface morphology, (iii) elemental content (iv) crystallinity properties and

(v) N₂ gas adsorption-desorption isotherm. The thermal properties characterization was conducted through the use of Thermogravimetry Analysis (TGA) method at a temperature of 600 °C and a gas flow rate of 10 °C min⁻¹. The N₂ gas adsorption-desorption isotherm was conducted by using the Quantachrome TouchWin v.1.2 instrument.

Furthermore, the specific surface area was evaluated by BET method while the BJH (Barrett-Joyner-Halenda) method was used for pore size distribution. Surface morphology and elemental content were characterized by using Scanning Electron Microscopy and Energy Dispersive X-ray with the Jeoul JSM 6510 LA instrument. Moreover, the crystallinity properties were investigated through the use of X-ray diffraction method with the Shimadzu 7000 instrument (source of CuKα with λ = 0.154 nm) at the scattering angles (2θ) of 10-60°.

2.3. Electrochemical properties

The electrochemical properties of carbon electrodes were characterized using the Cyclic Voltammetry method with a two-electrode system. They were measured through the use of a CV UR Rad-Er 5841 instrument at 1, 2, 5 and 10 mV s⁻¹ scan rate variations with a potential window of 0-1 V in 1 M H₂SO₄ electrolyte solution and the use of eggshell membrane as separator [7]. However, the specific capacitance was calculated using the following equation [8,9]:

$$C_{sp} = \frac{I_c - I_d}{sxm} \quad (1)$$

Where I_c is the charge current (A), I_d is the discharge current (A), s is the scan rate and m is the electrode mass.

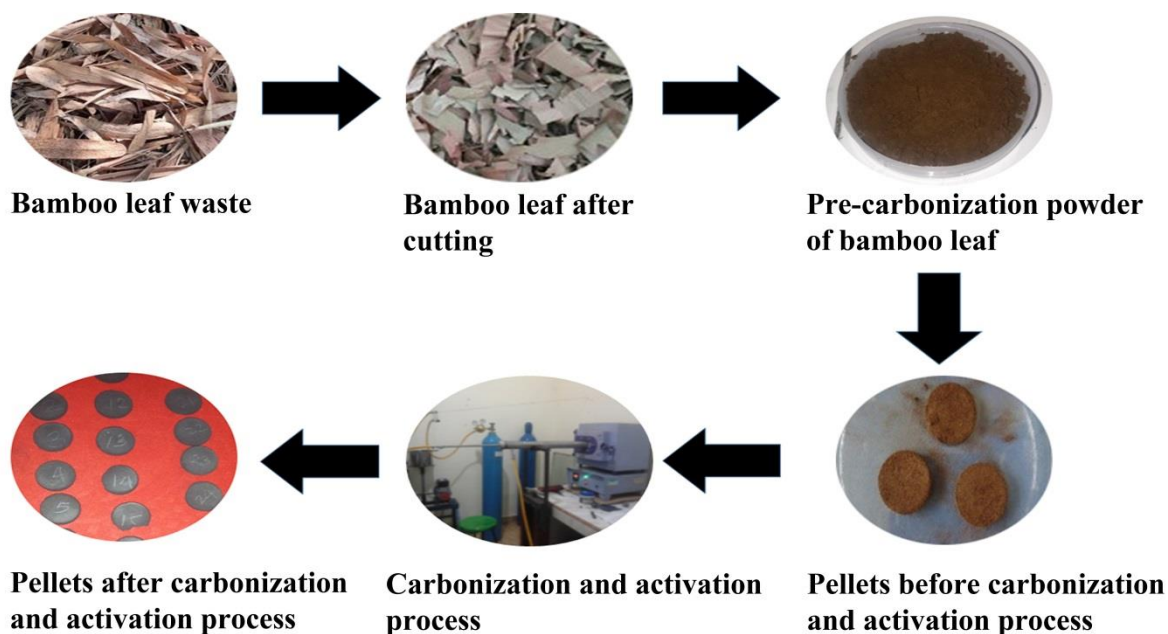


Figure 1. Preparation of the activated carbon from bamboo leaf

3. RESULTS AND DISCUSSION

3.1. Thermogravimetry analysis

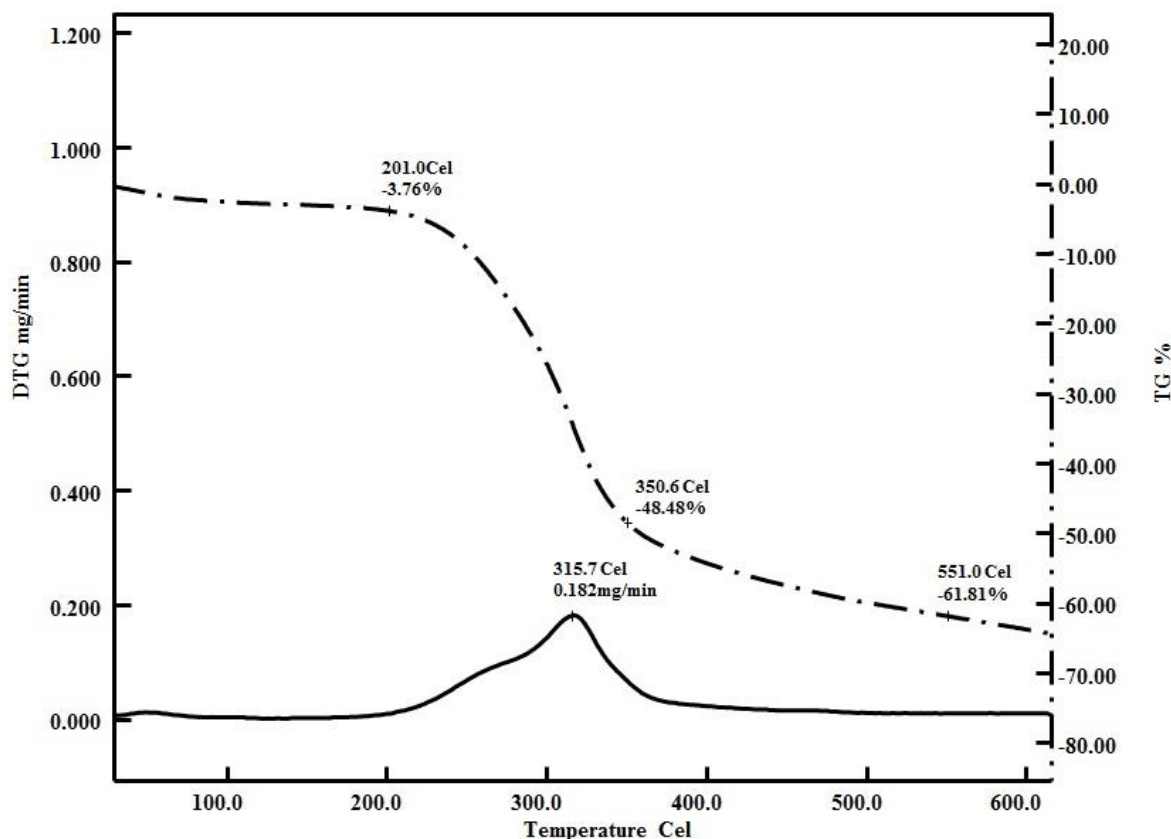


Figure 2. TG and DTG profile for bamboo leaf samples

The thermal stability for the pre-carbonized bamboo leaf is shown by the TG and DTG profile in Figure 2. TG and DTG analyses were conducted in the N_2 gas atmosphere at a temperature of 30–600 °C with an initial sample mass of 2.80 mg. TG profile shows the mass percentage reduction vs temperature while the DTG profile determines the reduction of mass per time vs temperature. The TG profile reveals the Pre-carbonized sample lost about 61.81% of mass before it reached 600 °C through 3 decomposition stages. The first stage occurred at a temperature of 100–200 °C with a mass decrease of 3.76% through the evaporation of moisture content [10]. The pyrolysis effect on the sample showed the highest mass loss of 44.72% in the second stage at a temperature of 250–400 °C. At this stage, there was a decomposition of complex compounds such as cellulose, hemicellulose, and lignin, as reported in the literature [11]. Furthermore, the samples decreased by 13.33% in the final stage at a temperature of 400–600 °C where the lignin compound decomposed as mentioned in the literature [12]. The highest decomposition rate on the DTG profile was $0.182 \text{ mg min}^{-1}$ as observed at about 315.7 °C indicating a broad peak. This is compatible with what was observed at the second stage of the TG profile and it can be said that 315.7 °C is the thermal resistance temperature for the bamboo leaf. However, it is important to point out that the analysis was simultaneously influenced by the reduction of complex

compounds. Therefore, the observed temperature is the standard for mass decomposition for carbon made from biomass material, as seen in rubber seed [13], date palm [14] and durian shell [12].

3.2. Crystallinity analysis

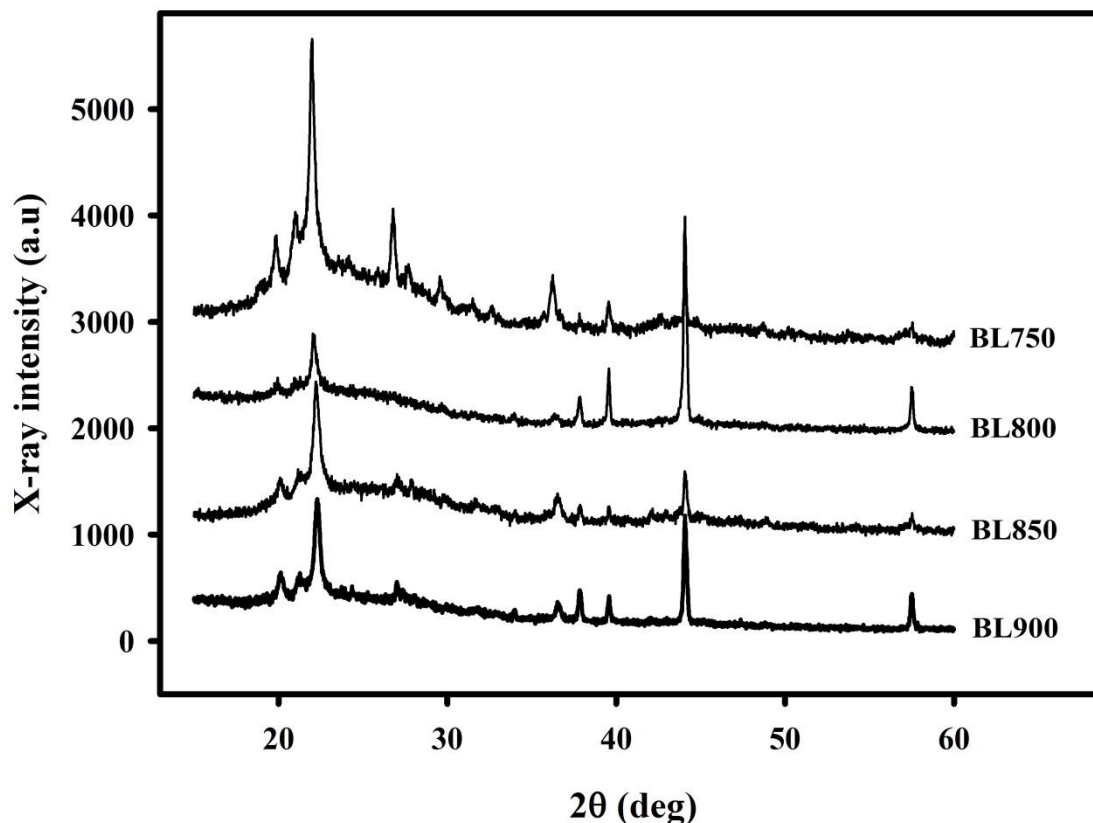


Figure 3. XRD pattern for all samples

Table 1. Diffraction peaks, interlayer spacing (d_{002} and d_{100}) and microcrystallite dimensions (L_c and L_a)

Sample code	2θ (002)	2θ (100)	d_{002} (Å)	d_{100} (Å)	L_a (Å)	L_c (Å)	L_c/L_a
BL750	21.9686	44.0425	4.0427	2.0544	12.6434	8.6185	0.6817
BL800	22.1476	44.0516	4.0105	2.0540	27.0333	12.9778	0.4801
BL850	22.2377	44.0551	3.9944	2.0538	10.5099	6.7457	0.6418
BL900	22.2802	44.0592	3.9869	2.0537	14.3462	8.7162	0.6076

The structures and surface chemistry of the Activated carbon made from bamboo leaf were analyzed by using X-ray diffraction (XRD) as shown in Figure 2 and two broad peaks were observed at 22° and 44° to represent the amorphous character of the carbon [15]. The broad peak at 22° was apparent in all samples, indicating the characteristic peak of graphite (002) plane attributed to the parallel stacking of flake graphite layers. The small peak observed at 44° indicates the (100) plane in

the hexagonal structure of pyrolytic carbon [16, 17]. The real diffraction peaks, interlayer spacing (d_{002} and d_{100}) and microcrystallite dimensions (L_c and L_a) are shown in Table 1. The interlayer spacing was calculated by using Bragg's equation [18] while the microcrystallite dimensions (L_c and L_a) were evaluated through the use of Debye-Scherrer equation [19, 20]. The interlayer spacing revealed the systematic trend to be correlated with while varying activation temperature. This is important because increasing the activation temperatures causes a decrease in interlayer spacing but do not show any systematic change in microcrystallite dimensions. The L_c and L_a observed in this study were similar to the those reported in previous research, for example, the activated carbon from oil palm empty fruit bunch [21]. However, the relationships between these two characteristics can be used to determine the specific surface area of XRD [22, 23]. $SSA_{xrd} = 2/(\rho_{xrd} L_c)$ where ρ_{xrd} was evaluated by using $\rho_{xrd} = (d_{002(\text{graphite})}/d_{002}) \rho_{(\text{graphite})}$ and $d_{002(\text{graphite})}$ and $\rho_{(\text{graphite})}$ were 0.33354 nm and 2.268 g cm⁻³, respectively [23]. Based on this relationship, BL850 has the largest surface area and this affects the electrochemical performance of supercapacitors. In agreement to this, there are many reports on the interrelation between interlayer spacing and microcrystallite dimension when evaluating the surface area and performance of super-capacitating cell [24, 25]. Moreover, L_c/L_a ratio represents the relative density of edge and basal planes in the microcrystallites and it was found to be regularly decreasing for all samples, except BL800.

3.3. Morphology area analysis

The effect of activation temperature on the surface morphology was analyzed by using Scanning Electron Microscopy method. The images of the BL750, BL800, BL850 and BL900 samples at a 5000x magnification are shown in Figures 4a, b, c, and d, respectively. The samples were discovered to exhibit a highly irregular shape and rough surface. Furthermore, the dark-bright morphology showed the presence of pores between the carbon particles while a bright pattern indicates the presence of particles on the surface of the sample. In Figure 4a, the particle sizes 0.248 to 0.401 μm for the sample was found to exhibit pores between 0.320-0.910 μm . Moreover, the increasing activation temperature in BL800 and BL850 samples as shown in Figures 4b and c caused the particle size to increase up to 0.348-1.068 μm and 0.350-1.50 μm , respectively. This is because higher activation temperatures leave more pores on the surface, resulting in less rigidity, and slightly increase particle size. The phenomenon can also be associated with the washing away of small-sized particles while the larger ones were left in the higher activation temperature of the sample. Moreover, the loss of small particles also allows increased pore size between particles in the BL900 sample to range from 0.63 to 4.03 μm as shown in figure 4d. Figures 2a, b, and d showed surface morphology samples with dominant macropores to be between 0.63 and 4.03 μm . However, the BL850 sample has a slightly different surface morphology compared to others because it looks denser. This sample has a relatively smaller pore size and this was further supported by data from N₂ adsorption-desorption gas which showed the similar result as well as the cyclic voltammetry measurement where the sample has the highest specific capacitance.

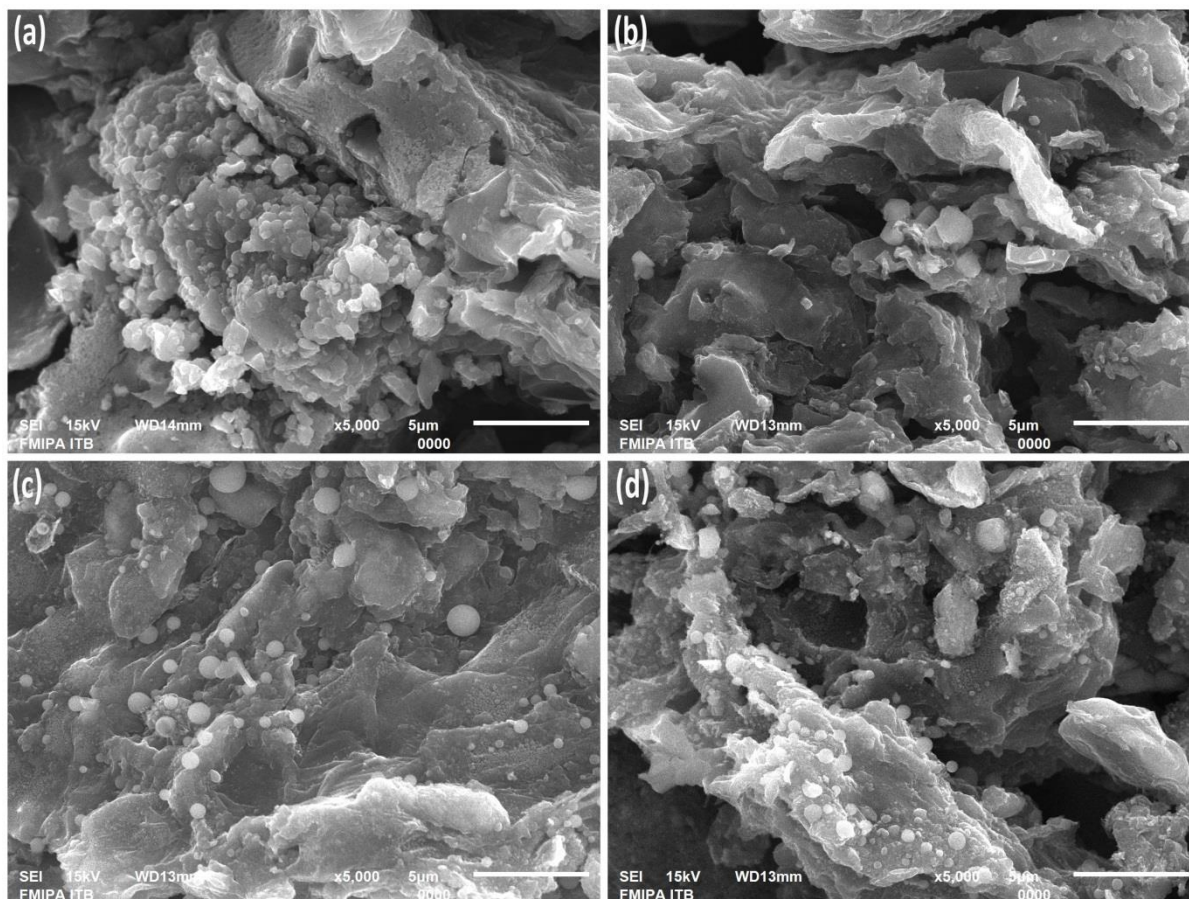


Figure 4. The SEM image with 5000x of magnification for a) BL750; b) BL800; c) BL850 and d) BL900 samples

3.4. Chemical content analysis

Table 2. The chemical content for carbon electrode samples

Chemical content	BL750		BL800		BL850		BL900	
	Mass	Atom	Mass	atom	Mass	atom	Mass	Atom
Carbon	66.14	75.31	77.30	83.83	77.75	84.90	69.94	78.84
Oxygen	23.01	19.67	16.65	13.55	14.44	11.84	19.47	16.48
Magnesium	0.30	0.17	0.20	0.11	0.34	0.19	0.31	0.17
Aluminium	0.31	0.15	-	-	-	-	-	-
Silicon	8.15	3.97	4.36	2.02	4.45	2.08	7.04	3.39

The chemical composition of the activated carbon made from the bamboo leaf is as shown in Table 2. It was discovered that the samples are made of carbon, oxygen, magnesium, aluminum, silica, chlorine, potassium and calcium with the carbon element dominating followed by oxygen. The oxygen is present because of the effects of the physical activation process while other elements such as silica, potassium, and calcium are the original elements of bamboo leaf. The activation temperature has an effect on the percentage of carbon in each sample by regularly increasing the content by 75-84%. In addition, other impurity elements were also degraded to produce high carbon purity as seen in the

BL850 sample which has the highest carbon content and the least chemical composition among the samples. This is in agreement with the reports of other pieces of literature [26, 27]. BL850 was found to have shown good physical properties of an electrode and also exhibited the highest specific capacitance.

3.5. The nitrogen adsorption isotherm analysis

The isothermal adsorption-desorption nitrogen gas and pore size distribution analysis of all samples are as shown in Figure 5. The method is popular for the evaluation of the porous nature and surface area of activated carbon.

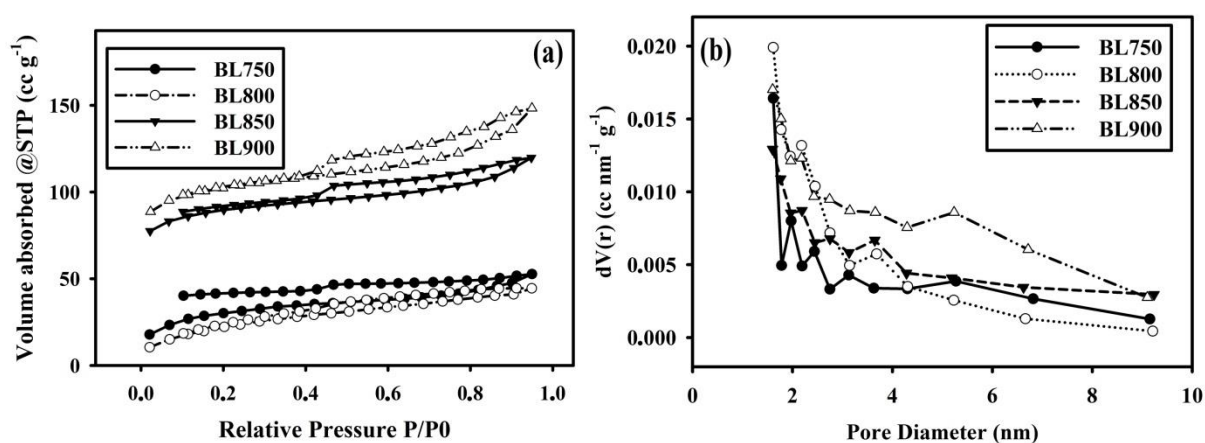


Figure 5. a) Nitrogen adsorption-desorption isotherms; b) Pore size distribution curves for all samples

Figure 5a showed the samples exhibited loop hysteresis with similarity to the type-IV based IUPAC classification which indicates the presence of the combination of micro and mesoporous in the samples [28, 29]. At a relatively low temperature of 0-0.4, micropore formation naturally occurs and when the pressure $P/P_0 > 0.4$ mesopores is exhibited by a hysteresis loop. Furthermore, the use of CO_2 activation agents allows the pores to develop well with the mesopores occurring in a higher percentage than micropores [30]. However, the addition of activation temperature shows a systematic increase in specific surface area of the sample to be $104.355 \text{ m}^2 \text{ g}^{-1}$, $83.246 \text{ m}^2 \text{ g}^{-1}$, $287.848 \text{ m}^2 \text{ g}^{-1}$, and $328.814 \text{ m}^2 \text{ g}^{-1}$ for BL750, BL800, BL850, and BL900, respectively. Moreover, the pore size distribution as shown in Figure 5b to concentrate on the diameter of 1-2 nm. Nevertheless, the real values were evaluated by Barret-Joyner-Halenda (BJH) to be 1.56 nm, 1.66 nm, 1.29 and 1.39 nm for BL750, BL800, BL850, and BL900, respectively.

3.6. Electrochemical performance analysis

The cyclic voltammetry measurement was used to test the electrochemical performance level of the supercapacitor. It generated the current charge and discharge data against certain potentials in order to evaluate the electrode specific capacitance. The CV curve of the constant scan rate (1 mV s^{-1}) is as revealed in Figure 6a. All the samples were shown to have a rectangular shape, which is the ideal shape of carbon material electrodes and this reflected the capacitance characteristic for supercapacitor cell [31]. However, the largest rectangular shape means the highest current charge while the lowest discharges and when this is connected to equation 1, the highest specific capacitance is achieved. Therefore, Figure 5a shows BL850 sample to have the highest specific capacitance.

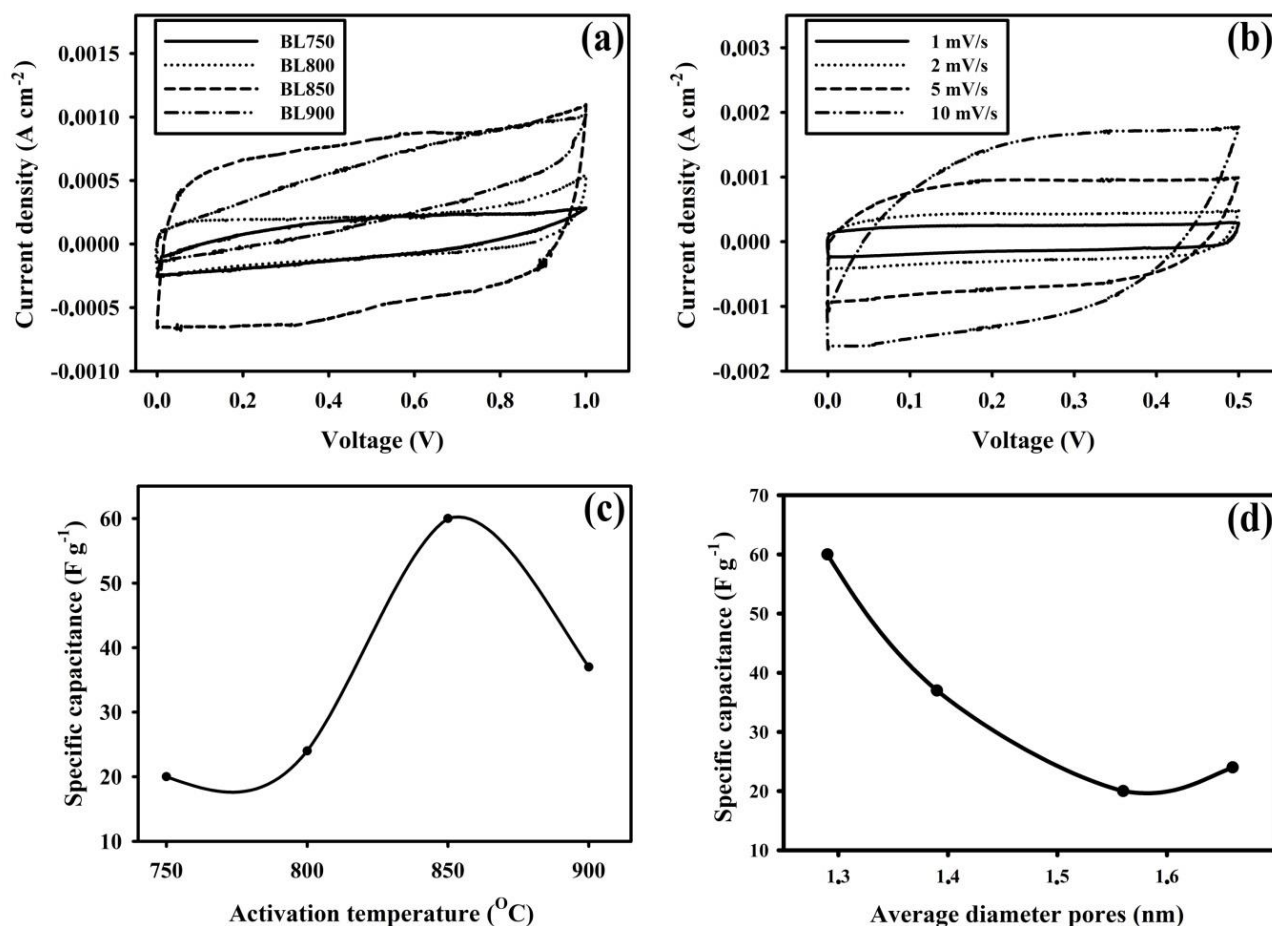


Figure 6. a) The CV curve for all samples; b) the variation of scan rate for BL850 sample; c) the relationship between specific capacitance with activation temperature; and d) The relationship between specific capacitance with an average pore diameter

Furthermore, the activation temperature was discovered to have effects on the electrode specific capacitance. Figure 6b shows the CV curve of BL850 sample at a different scan rate from 1 mV s^{-1} to 10 mV s^{-1} and it was observed to change frequently as the scan rate increases from a rectangular to a quasi-rectangular shape. The second shape indicates the surface has a well-developed

combination of micro and mesopores structure as found in the N₂ gas absorption analysis. Moreover, the specific capacities of different activation temperature from all samples are shown in Figure 6c and they were found to be frequently increasing from 750 °C to 850 °C and decreased afterward. The values were 20 F g⁻¹, 24 F g⁻¹, 60 F g⁻¹, and 37 F g⁻¹ for BL750, BL800, BL850, and BL900 samples, respectively. Therefore, the BL850 sample with an activation temperature of 850 °C possessed the maximum specific capacitance. This specific capacitance is almost the same as the other electrodes with similar materials for supercapacitors which shown in Table 3. An increasing activation temperature allows the electrode to have a lot of pores resulting in a high surface area as observed in the value of 104-380 m² g⁻¹ obtained for 750-900 °C respectively. However, the average pore diameter changed irregularly with BL850 having the smallest at 1.29 nm. This electrode showed the highest specific capacitance with low surface area and this means the capacitance characteristic was optimum in the pores. Therefore, it can be concluded that the activation temperature of 850 °C is the optimum temperature to prepare supercapacitor cells from bamboo leaf-based electrodes. In general, the relationship between specific capacitance and average pore sizes in the supercapacitor device is as shown in Figure 6d. It has been revealed that the electrode with pore sizes smaller than 1.5 nm tend to follow the EWCC model while those higher than 1.5 nm follow the EDCC model and limitation of each has been stated in Figure 6d.

Table 3. The comparison of specific capacitance for different biomass material as electrodes for supercapacitor

Biomass	Specific capacitance (F g ⁻¹)	References
Bamboo	60	32
Pandanus leave	56	33
Terminalia Catappa leaf (TCL)	54	34
Banana fiber	74	35
Sawdust	80	36

4. CONCLUSION

It can be concluded that several average pore diameters between 1.29 nm and 1.66 nm have been produced based on different characterizations and analyses conducted. The specific capacitance supercapacitor cell was also found to be closely related to the surface area and the average pore diameter size. Furthermore, the surface area is directly proportional to the activation temperature but the specific capacitance showed a slightly different trend at temperatures higher than 850 °C where irregularity was observed with the average pore size. Moreover, for electrodes with pore sizes smaller than 1.5 nm, the specific capacitance is inversely proportional to the average pore size while for those higher than 1.5 nm, it is directly proportional. Finally, a turning point (the validity limits of the EWCC and EDCC models) was found between specific capacitances and average pore size of carbon electrode in a supercapacitor device.

ACKNOWLEDGEMENTS

The author would like to thank the DRPM Kemenristek-Dikti through the doctor dissertation program of 2018 with the title “characteristics of activated carbon as a dielectric material for application of supercapacitor”. The author also thanks the SEM FMIPA ITB Laboratory, which has assisted in obtaining the SEM and EDX data.

References

1. M. Inagaki, H. Konno, O. Tanaike, *J. Power Sources*, 195 (2010) 7880
2. C-C Huang, Y-Z Chen, *J. the Taiwan Institute of Chemical Engineers*, 44 (2013) 611
3. L. Yin, Y. Chen, D. Li, X. Zhao, B. Hou, B. Cao, *Materials and Design*, 111 (2016) 44
4. E. Taer, R. Taslim, W. S. Mustika, B. Kurniasih, Agustino, A. Afrianda, Apriwandi, *Int. J. Electrochem. Sci.*, 13 (2018) 8428
5. J. Huang, B. G. Sumpter, V. Meunier, *Chem. Eur. J.*, 14 (2008) 6614 – 6626
6. E. Taer, Apriwandi, Yusriwandi, W.S. Mustika, Zulkifli, R. Taslim, Sugianto, B. Kurniasih, Agustino, P. Dewi, *AIP Conf. Proc.*, 1927 (2018) 030036-1
7. E. Taer, Sugianto, M.A. Sumantre, R. Taslim, Iwantono, D. Dahlan, M. Deraman, *Adv. Materials Research*, 896 (2014) 66.
8. E. Taer, R. Taslim, Z. Aini, S. D. Hartati, W. S. Mustika, *AIP Conf. Proc.*, 1801 (2017) 040004-1
9. E. Taer, P. Dewi, Sugianto, R. Syech, R. Taslim, Salomo, Y. Susanti, A. Purnama, Apriwandi, Agustino, R. N. Setiadi, *AIP Conf. Proc.*, 1927 (2018) 030026-1
10. L. L. Zhang, S. X. Zhao, *Chemical Society Reviews*, 38 (2009) 2520.
11. M. Brebu, C. Vasile, *Cellulose Chemistry Technology*, 49 (2010) 353.
12. E. Taer, A. Apriwandi, R. Taslim, U. Malik, Z. Usman, *Int. J. Electrochem. Sci.*, 14 (2019) 1318.
13. Kang, J. Jianchun, *Biomass and bioenergy*, 34 (2010) 539.
14. M. Shoaib, H. M. Al-Swaidan, *Biomass and bioenergy*, 73 (2015) 124
15. Wenxin Cao, Fuqian Yang, *Materials Today Energy*, 9 (2018) 406.
16. M. Liu, L. Gan, W. Xiong, F. Zhao, X. Fan, D. Zhu, Z. Xu, Z. Hao, L. Chen, *Energy Fuel*, 27 (2013) 1168.
17. Y. J. Hwang, S.K. Jeong, J. S. Shin, K. S. Nahm, A. M. Stephan, *J. Alloys Compd.*, 448 (2008) 141.
18. F. Li, W. Chi, Z. Shen, Y. Wu, Y. Liu, H. Liu, *Fuel Process Technol.*, 91 (2010) 17.
19. B. D. Cullity, *Elements of X-Ray Diffraction*, Ed. 3, (2001) Amazon Prentice Hall.
20. P. J. M. Carrott, J. M. V. Nabais, M. M. L. R. Carrott, J. A. Pajares, *Carbon*, 39 (2001) 1543.
21. R. Farma, M. Deraman, Awitdrus, I. A. Talib, R. Omar, J. G. Manjunatha, N. H. Basri, B. N. M. Dolah, *Int. J. Electrochem. Sci.*, 8 (2013) 257.
22. K. Kumar, R. K. Saxena, R. D. Kothari, K. Suri, N. K. Kaushik, J. N. Bohra, *Carbon*, 35 (1997) 1842.
23. M. Deraman, R. Daik, S. Soltaninejad, N. S. M. Nor, Awitdrus, R. Farma, N. F. Mamat, N. H. Basri, M. A. R. Othman, *Adv. Materials Research*, 1108 (2015) 1.
24. D. Qu, *J. Power Sources*, 109 (2002) 403.
25. Ch. Emmenegger, Ph. Mauron, P. Sudan, P. Wenger, V. Herman, R. Gallay and A. Zuttel, *J. Power Sources*, 124 (2003) 321.
26. M. Yu, Y. Y. Han, J. Li, L. J. Wang, *Chemical Engineering Journal*, 317 (2017) 493
27. M. Shoaib, H. M. Al-Swaidan, *Biomass and bioenergy*, 73 (2015) 124
28. W. S. K. Sing, H. D. Everett, W. A. R. Haul, L. Moscou, A. R. Pierotti, J. Rouquerol, T. Siemieniewska, *Pure & App. Chem.*, 57 (1985) 603.
29. K. Yu, H. Zhu, H. Qi, C. Liang, *Diamond & Related Materials*, 88 (2018) 18.
30. C-H. Ooi, T. Lee, S-Y. Pung, F-Y. Yeoh, *ASEAN Engineering Journal Part B*, 4 (2013) 40.

31. H. Chen, Y-c. Guo, F. Wang, G. Wang, P-r. Qi, X-h. Guo, F. Yu, B. Dai, *New Carbon Materials*, 32 (2017) 592.
32. C. Kim, J. W. Lee, J. H. Kim, K. S. Yang, *Korean J. Chem. Eng.* 23 (2006) 592.
33. E. Taer, A. Apriwandi, Krisman, Minarni, R. Taslim, A. Agustino, A. Afrianda, *J. Phys.: Conf. Ser.* 1120 (2018) 012006.
34. E Taer, A Afrianda, R Taslim, Krisman, Minarni, A Agustino, A Apriwandi, U Malik, *J. Phys.: Conf. Ser.* 1120 (2018) 012007.
35. Subramanian, C. Luo, A.M. Stephan, K.S Nahm, S. Thomas B. Wei, *J. Phys. Chem. C.*, 111 (2007) 7527.
36. W-J. Liu, K. Tian, Y-R. He, H. Jiang, H-Q. Yu, *Environ. Sci. Technol.*, 48 (2014) 13951.

© 2019 The Authors. Published by ESG (www.electrochemsci.org). This article is an open access article distributed under the terms and conditions of the Creative Commons Attribution license (<http://creativecommons.org/licenses/by/4.0/>).